Optics Letters

Construction of arbitrary vortex and superoscillatory fields

Matt K. Smith[1,*] and Gregory J. Gbur[2]

[1]Nanoscale Science Ph.D. Program, University of North Carolina at Charlotte, Charlotte, North Carolina 28223, USA
[2]Department of Physics and Optical Science, UNC Charlotte, Charlotte, North Carolina 28223, USA
*Corresponding author: msmit473@uncc.edu

Received 7 July 2016; revised 26 September 2016; accepted 27 September 2016; posted 28 September 2016 (Doc. ID 269616); published 25 October 2016

Superoscillations, oscillations of a bandlimited signal at frequencies greater than its band limit, have been verified both theoretically and experimentally. The design of such superoscillatory waves, however, has typically relied on complicated mathematics. We introduce a simple Fourier method to construct superoscillations in the transverse plane of an optical field in the form of optical vortices.

OCIS codes: (260.6042) Singular optics; (050.4865) Optical vortices; (050.1970) Diffractive optics.

http://dx.doi.org/10.1364/OL.41.004979

In Fourier analysis, it was long assumed that the fastest oscillations that could occur in a bandlimited signal could have a period no shorter than $2\pi/\omega_L$, where ω_L is the highest nonzero frequency of the signal. In the past 20 years, however, it has been shown that a signal can oscillate arbitrarily fast in the presence of closely spaced zeroes. Berry was the first to draw broad attention to this [1], and these so-called superoscillations have been investigated in the fields of quantum mechanics [2,3], signal processing [4,5], and optics [6–8].

Superoscillations have been shown to exist in the transverse plane of monochromatic optical fields in the presence of optical vortices [7]. Vortices are zero intensity lines in a three-dimensional space, at which the phase is undefined, or singular. About these singularities, the phase has a circulating or helical form [9]. Because of the analyticity of the wavefield, the phase can only change by an integer multiple of 2π in a circuit about the singularity [10, p. 228]. Investigations of these vortices and other singular structures have led to a new subfield of optics known as singular optics [10].

The most well-known beams possessing optical vortices are the Laguerre–Gauss beams of order p, l, where p and l are integers. In cylindrical coordinates, such a Laguerre–Gauss beam can be expressed in the waist plane ($z = 0$), without normalization, as [11, p. 649]

$$E_{\mathrm{LG}}(\rho,\phi) = E_0 \left(\frac{\sqrt{2}}{w_0}\right)^{|l|} L_p^{|l|}\left(\frac{2\rho^2}{w_0^2}\right) \exp\left(\frac{-\rho^2}{w_0^2}\right) \rho^{|l|} \exp(\pm i|l|\phi), \tag{1}$$

where w_0 is the beam width in the waist plane, E_0 is a constant, and $L_p^{|l|}$ denotes the associated Laguerre polynomials. It is worth noting that the last two terms can be combined and expressed in Cartesian coordinates to write

$$E_{\mathrm{LG}}(x,y) = E_0 \left(\frac{\sqrt{2}}{w_0}\right)^{|l|} L_p^{|l|}\left(\frac{2\rho^2}{w_0^2}\right) \exp\left(\frac{-\rho^2}{w_0^2}\right) (x \pm \mathrm{i}y)^{|l|}, \tag{2}$$

where $\rho^2 = (x^2 + y^2)$, and the plus/minus sign denotes a left-handed ($l > 0$) or right-handed vortex ($l < 0$), respectively, as demonstrated by the phase shown in Fig. 1.

Propagating fields that are naturally bandlimited in spatial frequency can have vortices arbitrarily close together, resulting in superoscillations. However, theoretical models of superoscillations typically use complicated mathematics, such as asymptotics [1] or Tschebyscheff polynomials [8], which can obscure the physics involved.

A more straightforward method using simple polynomials to construct superoscillations was recently developed by Chremmos and Fikioris for one-dimensional signals [12]. Their method was premised on the familiar property that the Fourier transform of powers of real-space variables results in differentiation in reciprocal space, i.e.,

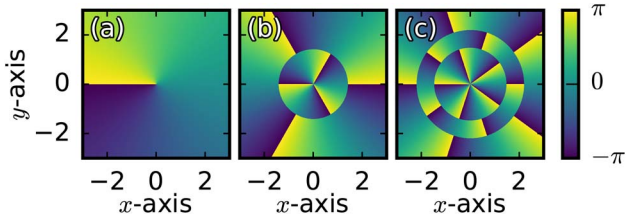

Fig. 1. Phase of a Laguerre–Gauss beam in Eq. (2), with $w_0 = 1$, $E_0 = 1$. (a) Left-handed, with $l = 1$, $p = 0$. (b) Right-handed, with $l = 3$, $p = 1$. (c) Left-handed, with $l = 5$, $p = 2$.

$$\mathcal{F}\{x^n f(x)\} = i^n \frac{d^n}{dk_x^n}\tilde{f}(k_x), \tag{3}$$

where $\mathcal{F}\{\}$ denotes the Fourier transform operator and $\tilde{f}(k_x)$ is the Fourier transform of $f(x)$. By using polynomials of x with roots at specified locations, they were able to create superoscillatory functions with arbitrarily many zeros packed arbitrarily close together. In this Letter, we extend this technique to two-dimensional fields and show that, in addition to making superoscillatory fields, it is also ideal for creation of arbitrary vortex arrangements in a given plane.

We begin with a bandlimited two-dimensional function in reciprocal space, $\tilde{f}(k_x, k_y)$, which has a corresponding real-space function $f(x, y)$, given by the inverse Fourier transform

$$f(x, y) = \frac{1}{(2\pi)^2}\iint_{-k_L}^{+k_L} \tilde{f}(k_x, k_y)\exp[+i(k_x x + k_y y)]\mathrm{d}k_x\mathrm{d}k_y, \tag{4}$$

where the limits of integration $-k_L$ and $+k_L$ are the band limits of our field. Let us multiply this real-space function $f(x, y)$ by an Nth-order polynomial $h(\tilde{z})$, where $\tilde{z} \equiv x + iy$. This polynomial is written as

$$h(\tilde{z}) = \sum_{n=0}^{N} a_n \tilde{z}^n, \tag{5}$$

where a_n are real constants. This yields a new function $g(x, y)$ of the form

$$g(x, y) = h(\tilde{z})f(x, y). \tag{6}$$

This real-space function will have the same band limits as $f(x, y)$, as shown by its Fourier transform,

$$\tilde{g}(k_x, k_y) = \sum_{n=0}^{N} a_n i^n[\partial_{k_x} + i\partial_{k_y}]^n \tilde{f}(k_x, k_y), \tag{7}$$

where ∂_{k_x} and ∂_{k_y} denote partial differentiation with respect to k_x and k_y, respectively. Since $\tilde{f}(k_x, k_y)$ is zero outside its band limits, the derivatives and constants a_n do not cause $\tilde{g}(k_x, k_y)$ to have greater bandwidth than $\tilde{f}(k_x, k_y)$. For $\tilde{g}(k_x, k_y)$ to avoid being singular (in the sense of delta distributions), however, the first $N - 1$ derivatives of $\tilde{f}(k_x, k_y)$ must be continuous [12]. This is required because each term of power n in the polynomial in $g(x, y)$ becomes a derivative of order n in the reciprocal space $\tilde{g}(k_x, k_y)$. Equation (3) showed this behavior for a real-space variable in one dimension.

If $h(\tilde{z})$ is chosen such that its zeros are closer together than the zeros of the fastest-oscillating component of $f(x, y)$, the resulting $g(x, y)$ will be superoscillatory in the region of those zeros. In other words, by choosing $h(\tilde{z})$ with roots at specified locations in the field $g(x, y)$, we can put zeros at arbitrary locations which, if they are close enough together, can result in superoscillations. In addition, since $g(x, y)$ has the $x \pm iy$ dependence of a vortex like Eq. (2) at these points, those points are optical vortices as well.

We note that this method could be physically implemented using a spatial light modulator (SLM) and a thin lens in a $2f$ focusing configuration, where f refers to the focal length of the lens. If the SLM is placed at the front focal plane of the lens and displays the reciprocal space field $\tilde{g}(k_x, k_y)$, then the image formed at the rear focal plane should correspond to the real-space field $g(x, y)$, since the two focal points are related via Fourier transform [13, p. 87].

To demonstrate the technique, we considered two choices for $\tilde{f}(k_x, k_y)$: the first we call *circular*, $\tilde{f}_{\mathrm{circ}}(k_x, k_y)$, and the second we call *rectangular*, $\tilde{f}_{\mathrm{rect}}(k_x, k_y)$. The functions are defined below:

$$\tilde{f}_{\mathrm{circ}}(k_x, k_y) = \cos\left(\frac{\pi}{2k_L}k\right)^5, \qquad k \equiv \sqrt{k_x^2 + k_y^2}, \tag{8}$$

$$\tilde{f}_{\mathrm{rect}}(k_x, k_y) = \cos\left(\frac{\pi}{2k_L}k_x\right)^6 \cos\left(\frac{\pi}{2k_L}k_y\right)^6. \tag{9}$$

In Eqs. (8) and (9), we define our band limits such that $\tilde{f}_{\mathrm{circ}}(k_x, k_y)$ is nonzero only for $|k| < k_L$, and $\tilde{f}_{\mathrm{rect}}(k_x, k_y)$ is nonzero only for $|k_x| < k_L$ and $|k_y| < k_L$. The functions $\tilde{f}_{\mathrm{circ}}(k_x, k_y)$ and $\tilde{f}_{\mathrm{rect}}(k_x, k_y)$ are so named because of their respective circular and rectangular symmetries about the origin.

For the polynomial $h(\tilde{z})$, we chose one for each $\tilde{f}(k_x, k_y)$. With $\tilde{f}_{\mathrm{circ}}(k_x, k_y)$, we used

$$h_{\mathrm{circ}}(\tilde{z}) = \tilde{z}^5 - \frac{5}{4}\tilde{z}^3 + \frac{1}{4}\tilde{z}, \tag{10}$$

which has roots at $\tilde{z} = 0, \pm 0.5$, and ± 1. With $\tilde{f}_{\mathrm{rect}}(k_x, k_y)$, we used

$$h_{\mathrm{rect}}(\tilde{z}) = \prod_{n=0}^{5} \mathcal{C}^n\{\tilde{z} - i\exp[i\pi(2n + 1)/6]\}, \tag{11}$$

which has roots forming a regular hexagon on the unit circle. Here, $\mathcal{C}$ is a complex conjugation operator. We use this operator to alternate the handedness of adjacent vortices.

The field $g(x, y)$ in the rear focal plane can be evaluated in two ways. The simplest is to use Eq. (4) to directly calculate $f(x, y)$, then multiply it by the appropriate polynomial $h(\tilde{z})$. For the rectangular case, $f_{\mathrm{rect}}(x, y)$ can be evaluated numerically by discretizing Eq. (4) or, alternatively, it can be evaluated analytically in the form

$$f_{\mathrm{rect}}(x, y) = \frac{1}{(2\pi)^2}\sum_{m=0}^{6}\sum_{j=0}^{6}\binom{6}{m}\binom{6}{j}\mathrm{sinc}[\beta_m(x)]\mathrm{sinc}[\beta_j(y)], \tag{12}$$

where $\beta_m(x) \equiv (6 - 2m)\pi/2 + xk_L$, and similarly for $\beta_j(y)$. We used both ways, and the root-mean-square difference between the resulting analytical $|g_{\mathrm{rect}}|$ and the numerical $|g_{\mathrm{rect}}|$ was less than 1.1×10^{-11}% of the mean value of $|g_{\mathrm{rect}}|$. The circular case does not have an analytical form to compare against.

In the SLM-based system mentioned earlier, however, the field $g(x, y)$ would be determined directly from the Fourier transform of $\tilde{g}(k_x, k_y)$, and $g(x, y)$ would be necessarily discrete due to the finite resolution of the SLM. It could not immediately be discounted that the superoscillations in the rear focal plane might be lost in the discretization of $g(x, y)$. Therefore, we also evaluated $g(x, y)$ by direct Fourier transform of $\tilde{g}(k_x, k_y)$ to compare with the first method of calculation. Due to the complexity of the derivatives in Eq. (7), we only did this comparison for a rectangular case with three zeros, located at $\tilde{z} = -1, 0, 1$. The root-mean-square difference between the normalized $|g_{\mathrm{rect}}|$ calculated by the two methods was less than 1.8×10^{-8}% of the mean of $|g_{\mathrm{rect}}|$, and the superoscillatory zeros were present in both cases.

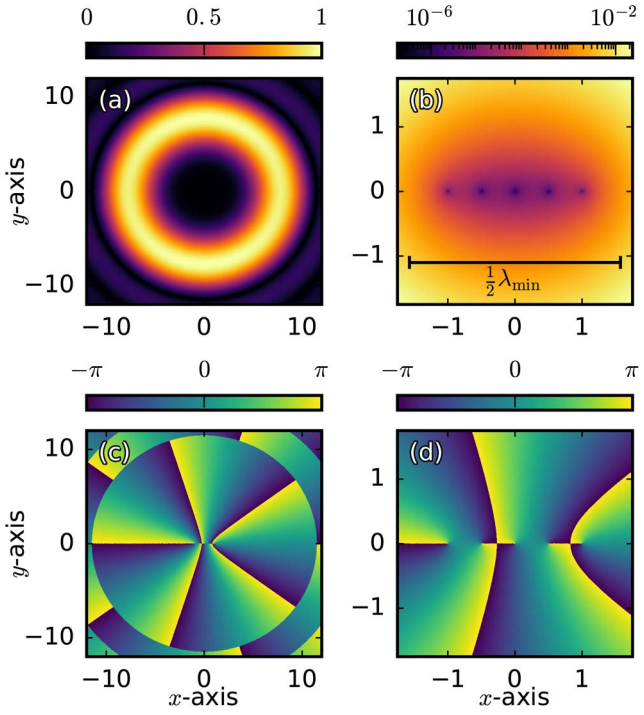

Fig. 2. Magnitude and phase plots for the circular case, with $k_L = 1$. (a) Normalized magnitude of g_{circ}. (b) Magnitude of g_{circ}, zoomed in to show the zeros at the roots of Eq. (10) and normalized to (a). Note the logarithmic scale. (c) Phase of the field in (a). (d) Phase of the field in (b).

All results shown in this Letter come from the first method of calculation, by discretizing Eq. (4), with 1001 points along each of the k_x and k_y axes. The calculations were done in the Python programming language using the tools in Refs. [14–17].

The resulting superoscillations and optical vortices for the circular case are depicted in Fig. 2. Figure 2(a) shows the normalized magnitude of g_{circ}, which roughly corresponds to the intensity, $|g_{\text{circ}}|^2$. It has a dark center surrounded by alternating bright and dark rings. Figure 2(b) shows the central dark spot of Fig. 2(a). The magnitude has been normalized to the maximum magnitude in Fig. 2(a) and plotted on a logarithmic scale. As expected, zeros can be seen at $\tilde{z} = 0, \pm 0.5$, and ± 1, the roots of Eq. (10). The reciprocal space function $\tilde{f}_{\text{circ}}(k_x, k_y)$ is bandlimited by $\pm k_L$, and $k_L = 1$ here, so we would typically expect no oscillations with a period $\lambda_{\min}$ less than 2π. However, since we have five zeros on a line from −1 to 1, which roughly corresponds to a period of 1, the field is superoscillatory along the line connecting the zeros. The magnitude of the field in the area of the superoscillations is about five orders of magnitude lower than the field in the circular region near it. This sort of behavior is to be expected, since the superoscillatory region of a field must be exponentially weaker than the nearby field [1]. The presence of optical vortices can be confirmed by examining the phase of the beam in Figs. 2(c) and 2(d). Figure 2(c) shows the phase of the field in Fig. 2(a). It has a similar pattern to the $l = 5$, $p = 2$ Laguerre–Gauss beam in Fig. 1(c). We can see that it has a discontinuity of π across the dark rings in Fig. 2(a) and that it undergoes five full 2π cycles about the central region, corresponding to the five roots of Eq. (10). These cycles are shown most clearly in Fig. 2(d),

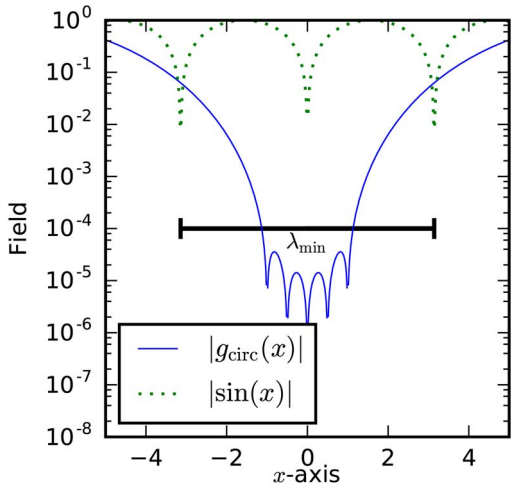

Fig. 3. x-axis of $|g_{\text{circ}}|$, with $k_L = 1$, plotted with a sinusoid of the minimum wavelength associated with this bandwidth. The thick black line is the wavelength of the sinusoid. Note the logarithmic scale.

which shows the phase of the zoomed-in region of Fig. 2(b). The phase makes a full 2π rotation about each of the roots of Eq. (10), confirming that these points are optical vortices.

The superoscillatory behavior of g_{circ} can be further shown by considering Fig. 3, which shows the x-axis of $|g_{\text{circ}}|$ and a sinusoid of the expected shortest wavelength, which is 2π. It is clear that the function g_{circ} undergoes oscillations more rapid than those of the sinusoid.

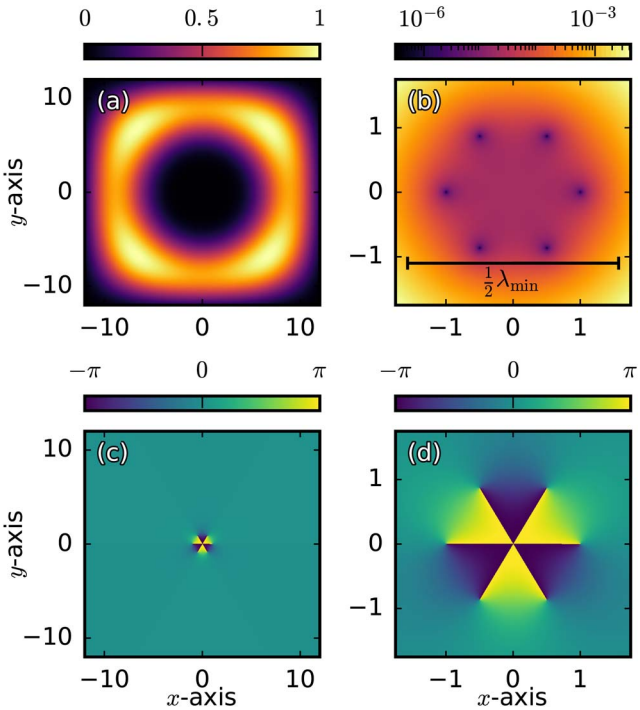

Fig. 4. Magnitude and phase plots for the rectangular case, with $k_L = 1$. (a) Normalized absolute value of g_{rect}. (b) Magnitude of g_{rect}, zoomed in to show the zeros at the roots of Eq. (11) and normalized to (a). Note the logarithmic scale. (c) Phase of the field in (a). (d) Phase of the field in (b).

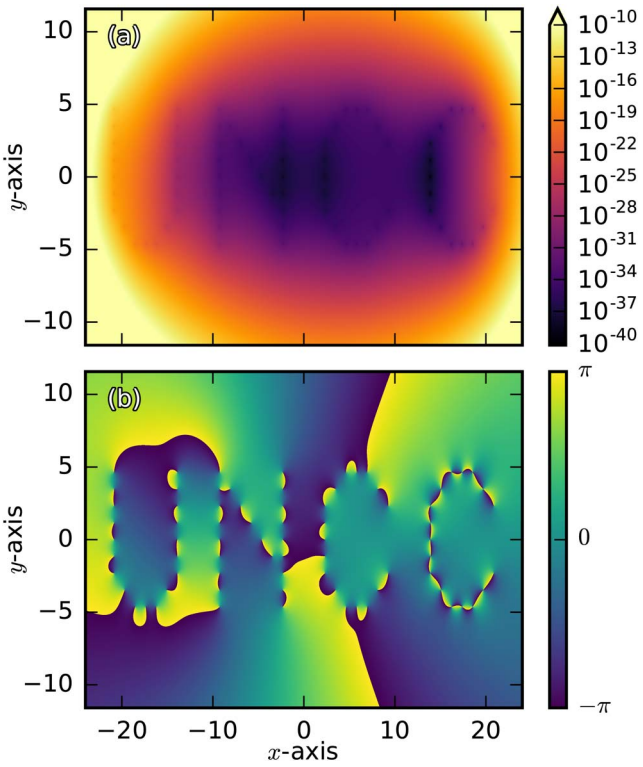

Fig. 5. Magnitude and phase plots for a field with vortices arranged to spell "UNCC." Each of the letters has alternating right-handed/left-handed vortices. The vortices in the second "C" are second order, with the exception of the end points. (a) Normalized magnitude of the field. To help make the vortices visible, the color map was capped at a maximum of 1×10^{-10}. (b) Phase of the field.

We see similar results for the rectangular case shown in Fig. 4. Figure 4(a) shows the normalized magnitude of g_{rect}, which consists of a dark central circle surrounded by a bright square. Figure 4(b) shows the magnitude of the dark region, scaled and plotted in the same way as Fig. 2(b). It can be seen that the field has zeros forming a regular hexagon on the unit circle, corresponding to the roots of Eq. (11). The phase of the field is shown in Figs. 4(c) and 4(d). Figure 4(c) shows the phase of the field in Fig. 4(a). In Fig. 4(d), we again see vortices at the roots of Eq. (11), confirming our ability to place vortices wherever we wish in the field. Additionally, it can be seen that the vortices are alternately right-handed and left-handed due to the complex conjugation we employed in $h_{\text{rect}}(\tilde{z})$.

An earlier method by Dennis [18] used phase perturbations of a high-order vortex field to produce lines and polygons of vortices similar to those of Figs. 2 and 4, and later was shown to produce superoscillations [19], but the method presented here has several distinct advantages. First, our polynomial method can produce vortices of any handedness in any arrangement, whereas the perturbation method can only make arrangements of the same handedness. Second, our method can place high-order vortices (of an order greater than unity) at any position in the observation plane. Third, our method has no restrictions on the placement of vortices, and is not restricted to the line and polygon configurations shown earlier. Finally, the inclination of the vortices can be arbitrarily chosen in our `method, by replacing the $x \pm iy$ dependence with an $ax \pm iy$ dependence. Doing so would produce mixed edge/screw vortices for which the vortex line is at an angle to the z-axis [20, p. 102].

Most of these advantages can be seen in Fig. 5, which depicts a field of 76 vortices arranged to spell "UNCC." The vortices in each letter alternate between left-handed and right-handed. The vortices in the second "C" are all second order, except for the endpoints. This field was made using $\tilde{f}_{\text{rect}}(k_x, k_y)$ from Eq. (9), except that the exponent used was 120 rather than 6, which is more than large enough to ensure that the required derivatives exist. The polynomial $h(z)$ was made by choosing vortex locations on a grid and making these locations the roots $\tilde{z}_r$ of the polynomial. The polynomial was finally constructed by multiplying terms $(\tilde{z} - \tilde{z}_r)$ together, applying conjugation where a left-handed vortex was desired and squaring where a second-order vortex was desired.

In conclusion, we have demonstrated a method that can be used to place optical vortices of arbitrary sign and order at arbitrary locations within a field, given that the reciprocal space function $\tilde{f}(k_x, k_y)$ has sufficient derivatives for the number of vortices. We have used here functions $\tilde{f}(k_x, k_y)$ which are continuously differentiable to order $N - 1$ and polynomials of order N. The result is that $\tilde{g}(k_x, k_y)$ is discontinuous at the edge of the domain. We may also use functions which are more continuous, which should result in less strong secondary oscillations of $g(x, y)$. It is to be noted that earlier work by Abramochkin and Volostnikov [21] used a related strategy to that described here to produce beams with geometric-shaped intensity patterns; that work, however, did not stress the positioning of vortices.

Funding. Air Force Office of Scientific Research (AFOSR) (FA9550-13-1-0009).

REFERENCES

1. M. Berry, *Quantum Coherence and Reality: in Celebration of the 60th Birthday of Yakir Aharonov*, J. S. Anandan and J. L. Safko, eds. (World Scientific, 1994), pp. 55–65.
2. M. S. Calder and A. Kempf, J. Math. Phys. **46**, 012101 (2005).
3. M. V. Berry and S. Popescu, J. Phys. A **39**, 6965 (2006).
4. A. Kempf, J. Math. Phys. **41**, 2360 (2000).
5. P. J. S. G. Ferreira and A. Kempf, IEEE Trans. Signal Process. **54**, 3732 (2006).
6. F. M. Huang, Y. Chen, F. J. Garcia de Abajo, and N. I. Zheludev, J. Opt. A **9**, S285 (2007).
7. M. R. Dennis, A. C. Hamilton, and J. Courtial, Opt. Lett. **33**, 2976 (2008).
8. A. M. H. Wong and G. V. Eleftheriades, IEEE Trans. Antennas Propag. **59**, 4766 (2011).
9. A. M. Yao and M. J. Padgett, Adv. Opt. Photon. **3**, 161 (2011).
10. M. Soskin and M. Vasnetsov, *Progress in Optics*, E. Wolf, ed. (Elsevier, 2001), Vol. **42**, Chap. 4, pp. 219–276.
11. G. J. Gbur, *Mathematical Methods for Optical Physics and Engineering* (Cambridge University, 2011).
12. I. Chremmos and G. Fikioris, J. Phys. A **48**, 265204 (2015).
13. J. W. Goodman, *Introduction to Fourier Optics* (McGraw-Hill, 1968).
14. K. J. Millman and M. Aivazis, Comput. Sci. Eng. **13**, 9 (2011).
15. J. D. Hunter, Comput. Sci. Eng. **9**, 90 (2007).
16. S. van der Walt, S. C. Colbert, and G. Varoquaux, Comput. Sci. Eng. **13**, 22 (2011).
17. F. Pérez and B. E. Granger, Comput. Sci. Eng. **9**, 21 (2007).
18. M. R. Dennis, Opt. Lett. **31**, 1325 (2006).
19. M. V. Berry, J. Opt. **15**, 044006 (2013).
20. J. F. Nye, *Natural Focusing and Fine Structure of Light* (IOP, 1999).
21. E. Abramochkin and V. Volostnikov, Opt. Commun. **125**, 302 (1996).